ORIGINAL PAPER

RJME
Romanian Journal of Morphology & Embryology
http://www.rjme.ro/

Three-dimensional organ scanning reveals brain edema reduction in a rat model of stroke treated with an aquaporin 4 inhibitor

ELENA SILVIA POPESCU[1)], IONICA PIRICI[2)], RALUCA NICULINA CIUREA[3)], TUDOR-ADRIAN BĂLŞEANU[4)], BOGDAN CĂTĂLIN[4)], CLAUDIU MĂRGĂRITESCU[3)], LAURENŢIU MOGOANTĂ[5)], SORIN HOSTIUC[6)], DANIEL PIRICI[7)]

[1)]*Department of Physiopathology II, "Carol Davila" University of Medicine and Pharmacy, Bucharest, Romania; "Prof. Dr. Matei Balş" National Institute for Infectious Diseases, Bucharest, Romania*

[2)]*Department of Anatomy, University of Medicine and Pharmacy of Craiova, Romania*

[3)]*Department of Pathology, University of Medicine and Pharmacy of Craiova, Romania*

[4)]*Department of Physiology, University of Medicine and Pharmacy of Craiova, Romania*

[5)]*Department of Histology, University of Medicine and Pharmacy of Craiova, Romania*

[6)]*"Carol Davila" University of Medicine and Pharmacy, Bucharest, Romania; "Mina Minovici" National Institute of Legal Medicine, Bucharest, Romania*

[7)]*Department of Research Methodology, University of Medicine and Pharmacy of Craiova, Romania*

Abstract

Stroke is one of the most important cause of death and disability, especially when considering the increasing life expectancy worldwide, with ischemic stroke being much more common than hemorrhages. In the physiopathological chain of ischemic stroke, brain edema is one first element that if attended to might reduce tissue necrosis, penumbra, and increase functional recovery. Aquaporin 4 (AQP4) has been found to be the most important water channel in the brain, and its inhibition before inducing focal ischemia in an animal model of stroke proved to alleviate the pathology and improve clinical recovery. In this study, we have treated a rat model of ischemic stroke with the AQP4 inhibitor TGN-020 after inducing the lesion, and performed for the first time a direct histopathological evaluation of the brain and infarct's volume. Besides utilizing immunohistochemistry targeting the growth-associated protein-43 (GAP-43) in order to delineate the infarct regions, we have used the Cavalieri's principle of tissue volume measurements starting form seriate sections, and for the first time in neuropathology, we have utilized a high-resolution object scanner to assess global brain volume changes. Our results showed that TGN-020 clearly reduces infarct volume in TGN-020 treated animals compared to untreated animals, as well as the volume of the brain hemispheres. Although reduced, the effect was also present in the contralateral hemisphere. Given these data, a more in-depth characterization of the histopathological and molecular changes induced by AQP-4 are needed for considering it as a *bona fide* treatment option.

Keywords: aquaporin 4, inhibitor, ischemic stroke, edema, rat model.

Introduction

Stroke is the fifth leading cause of death and represents a major cause of disability throughout the world [1]. Ischemic stroke results from a sudden loss of blood flow to an area of the brain, leading to a loss of neurological function. It is most frequently caused by thrombotic or embolic occlusion of a cerebral artery and represents up to 80% of all stroke patients [2, 3]. To date, the only Food and Drug Administration (FDA) approved physiopathologically-oriented treatments for ischemic stroke is the use of fibrinolytic and endovascular therapies.

For the most important acute complication of the hypoxic-ischemic event, edema, there is no pathogenically-oriented treatment. The only currently accepted non-surgical approach in the treatment of brain edema is represented by parenteral administration of hypertonic solutions, which lower intracranial pressure by shifting water from the brain parenchyma to the blood [4]. Brain edema can be mainly divided into: (*i*) an initial phase, or the cytotoxic edema, which occurs due to the incapacity of the cells to maintain the activity of their transmembrane adenosine triphosphate (ATP)-dependent Na^+/K^+ pumps in ischemic conditions, and which results in a net influx of Na^+, Cl^- and water towards the cytoplasms; and (*ii*) the so-called vasogenic edema, which is associated with the dysfunction of the brain blood barrier (BBB) in ischemic conditions leading to a progressive alteration of its permeability, leading to water inflow and eventually hemorrhagic transformation, especially if associated with vascular reperfusion [5]. Water diffusion in the brain is controlled by members of a water-channels-forming proteins family called aquaporins (AQPs). Aquaporin 4 is the most abundant form in the brain, is located mainly on the perivascular, subpial and subependymal membrane of the astrocytes, and acts like a bidirectional water channel depending on the local osmotic forces [6–8]. As a result, AQP4 knockout animal models resulted in opposite effects when these animals were subjected to either cytotoxic or vasogenic brain edema [9–12]. In an

ischemic model based on the middle cerebral artery occlusion (MCAO), the AQP4-/- background proved to be protective, improving the clinical outcomes and reducing brain swelling compared to wild-type animals [9].

Recent, *in vitro* and *in vivo* studies identified 2-(nicotinamide)-1,3,4-thiadiazole (TGN-020) as a potent AQP4 inhibitor [13–15]. Although the pretreatment with a single dose of TGN-020 showed potency in reducing brain edema in a mouse model of cerebral ischemia on magnetic resonance imaging (MRI), no histopathological study assessed directly these changes [14, 15].

To address this question, we utilized here the Cavalieri's principle of tissue volume extrapolating starting from systematically sampled seriate slides of the specimens, in order to directly evaluate the changes on the brain hemispheres' volumes in a rat model of ischemic stroke treated with TGN-020 after the induction of the lesion. Moreover, by utilizing the immunostaining for the growth-associated protein-43 (GAP-43) as a direct marker of the infarcted tissue, we have also evaluated the infarct volumes themselves. Finally, we have utilized for the first time in neuropathology a three dimensional scanner to evaluate the overall volumetric changes of these brains and to compare the effect of the TGN-020 treatment.

Materials and Methods

Animals

The study was performed on 21 male Sprague–Dawley rats ("Cantacuzino" National Institute of Research and Development for Microbiology and Immunology, Bucharest, Romania) of 3–4 months old [mean weight 425.26 g, standard deviation (SD) 32.61 g]. The animals were housed in groups of three in a controlled 12 hours light/12 hours dark schedule, and had *ad libitum* access to water and a standard pellet diet until the day before surgery.

Animals were randomly assigned to one of the four groups: (*i*) healthy control group (n=4), (*ii*) sham control group (n=6), (*iii*) untreated stroke group (n=5), and (*iv*) treated stroke group (n=6).

Surgery

Focal cerebral ischemia was induced by the permanent occlusion of the middle cerebral artery (MCA). The rats were anesthetized using a Ketamine/Xylazine cocktail (80–100 mg/kg / 5–10 mg/kg intraperitoneally), the head fixed in a stereotaxic device, and a small craniotomy was made in the temporal bone, above the MCA bifurcation. Under the surgical microscope, a 2 cm incision was made between the left orbit and the tragus, and a 3 mm diameter craniotomy was made just rostral to the foramen ovale [16]. The dura was incised and the distal MCA was exposed. After being lifted up with a tungsten hook attacked to micromanipulators, the MCA was cauterized with a Toolcraft ST-50D digital soldering station and a 0.2 mm soldering tip heated at 330ºC [17] (Figure 1).

The artery was coagulated in two points leading to a complete absence of the blood flow under the microscope. Body temperature was maintained at 37±0.5°C throughout the procedure using a homeothermic blanket. After surgery, the animals were placed on a 37°C warming tray, with food and water being accessible inside the cage. Sham animals had the craniotomy performed then the muscles and the skin were sutured.

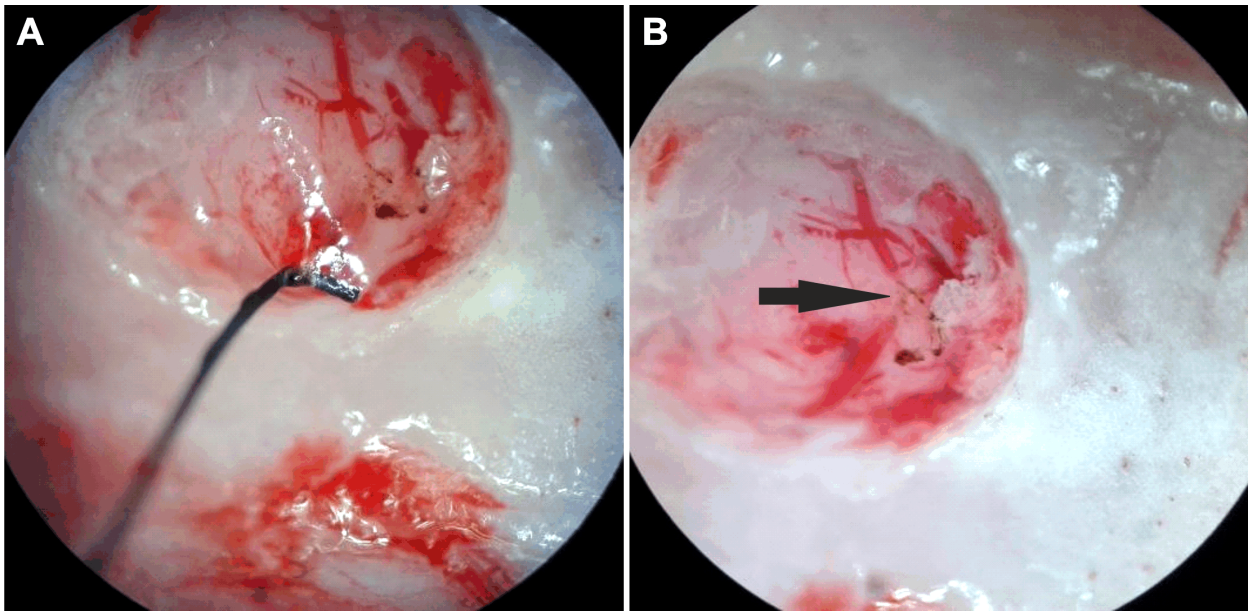

Figure 1 – ***Intra-surgery exemplary image showing the interruption (arrow) of the middle cerebral artery (MCA) after lifting it with a hook attached to a micromanipulator and its cauterization, (A) before and (B) after the hook retraction.***

TGN-020 preparation and treatment

As treatment option, the animals received a single intra-peritoneal injection, of TGN-020 hloride salt (Ukrorgsyntez Ltd., Kiev, Ukraine), 100 mg/kg, dissolved in 0.4 mL sterile distilled water and tittered with 1 M sodium hydroxide until a pH of 8, at 15 minutes after the induction of MCAO. This concentration was deemed above the physiologically effective values, as reported by other studies [14, 18, 19]. Untreated MCAO animals received the same volume of isotonic saline. Sham operated animals

were only anesthetized and the skulls drilled to expose the MCA.

Tissue processing and whole brains *ex vivo* scanning

After a survival time of three days, the animals were deeply anesthetized, hearts were perfused with saline, 10% neutral buffered formalin, and the organs were harvested and further fixed for two days at room temperature. All organs have been sectioned to allow a better fixation, and the brains were cut frontally at bregma levels +2 mm, and –3 mm [20]. Before sectioning, the fresh brains were mounted vertically on a custom made holder, placed on the scanner tray of an EinScan-S white light three-dimensional (3D) scanner (Shining 3D, Zhejiang, China), and complete high resolution 3D surface scan StereoLithography (**.stl*) files were generated for each specimen in the EinScan software. Moreover, in order to test for intra-sample variations, each brain was re-positioned on the scanning table and a second scan was performed.

All tissues were then processed for paraffin embedding and then cutting on a rotary microtome HM355S with a waterfall-based section-transfer system (Thermo Scientific Inc., Walldorf, Germany). For the brain, the 5 mm-thick tissue block containing the stroke volume was completely cut as series of 10×5 μm thick sections followed by 10×20 μm thick sections. Thin sections were picked from these series for each sample, prepared and analyzed following routine Hematoxylin and Eosin staining.

Immunohistochemistry

One 5 μm-thick section was randomly selected from the first series of 10×5 μm seriate sections, then representative thin sections were picked systematically at each 250 μm from each series of slides, with 15 such slides covering the entire volume of the infarct core. These representative sections were deparaffinized, rehydrated in graded alcohol series, subjected to antigen retrieval by microwaving in citrate buffer pH 6 for 20 minutes, incubated in 1% hydrogen peroxide in distilled water for 30 minutes to block the endogenous peroxidase activity, and kept for another 30 minutes in 3% skimmed milk in phosphate-buffered saline (PBS). The sections were next incubated at 4°C for 18 hours with a mouse anti-rat GAP-43 primary antibody (NBP-41337, diluted as 1:200, Novus Biologicals, UK), and the next day the signal was amplified for 30 minutes with an anti-mouse peroxidase polymer detection system adsorbed for rat immunoglobulins (Nikirei-Bioscience, Tokyo, Japan). The signal was finally detected with 3,3'-diaminobenzidine (DAB) (Dako, Glostrup, Denmark) and the slides were coverslipped in DPX (Sigma-Aldrich, St. Louis, MO, USA) after a Hematoxylin and Eosin staining. All slides were processed in the same time for protocol consistency together with negative control slides, which were obtained by omitting the primary antibodies.

Image and volumetric analysis

All the immunostained slides were scanned at 10× objective on a Nikon 90i microscope (Nikon Instruments Europe BV, Amsterdam, The Netherlands) equipped with a Prior OptiScan ES111 motorized stage (Prior Scientific, Cambridge, UK), a Nikon DS-5Mc cooled color camera and the Nikon NIS-Elements Advanced Research imaging and control software. Complete scanned coronal images were saved as non-compressed **.tiff* files and manual outlines were drawn to delineate each hemisphere and respectively the infarct core. After pixel-size calibration, all areas delineated by the contours were calculated and further utilized to estimate the hemispheric volumes and the infarct volumes utilizing the Cavalieri's method after the following formula: Volume (μm) = A×15×250, where 15 represents the total number of counted sections situated at 250 μm apart, and "A" represents the sum of the total areas of interest (thus calculated separately for the hemispheres and the infarct core respectively) [21–23].

Surface **.stl* files were processed in the Meshmixer 11.0.544 software (Autodesk Inc., San Rafael, CA, USA) for removal of the olfactory bulbs and cerebellum regions, between the bregma levels +5 mm, and –8 mm [20], and the brain volumes were calculated on the remaining data. Finally, all resulting data were plotted in Microsoft Excel as average ± SD (standard deviation of the means), and statistical differences were sought using a one-way ANOVA (analysis of variance) with the *post hoc* Fisher's LSD (least significant difference) test for multiple comparisons, in SPSS 10.0 (SPSS, Inc., Chicago, IL, USA). A value of $p<0.05$ was considered to be statistically significant.

Results

Except for one animal that died during the first night after the surgery, no animal deaths have been recorded in this experimental setup.

Histopathology analysis confirmed on all MCAO animals typical morphopathological changes associated with recent ischemic stroke (Figure 2, A, C and E). Microscopy revealed cellular contours loss, neuronal bodies shrinkage, chromatolysis of the Nissl bodies, eosinophilic cytoplasm, foamy appearance of the neuropil and irreversible nuclear changes, with a few foamy macrophages already present in the core of the infarct at this age (Figure 2C). Sparse gemistocitic astrocytes could also be noted around the lesion core (Figure 2D). Necrotic areas involved only the temporal cortex and did not cross the corpus callosum towards the thalamus and diencephalon. With the exception of occasional petechial small red blood cells extravasates, there was no massive hemorrhagic transformation in these animal model (Figure 2E).

Immunohistochemistry for the anti-GAP-43 antibody showed a strong and selective staining of the recent infarcted areas (Figure 2, B, F and H), with the signal being most prominent in the neuronal bodies and their apical dendrites (Figure 2F). The neuropil showed a diffuse less strong staining, with no clear-cut differentiation of other cellular processes. Foamy macrophages and endothelial cells stood out as not taking up the stain in the lesional tissue (Figure 2G), while some isolated perikarya were still stained around the necrotic tissue (Figure 2H). There was no difference in cellular localization and intensity of the staining between treated and non-treated MCAO animals, with no staining in control/sham tissue.

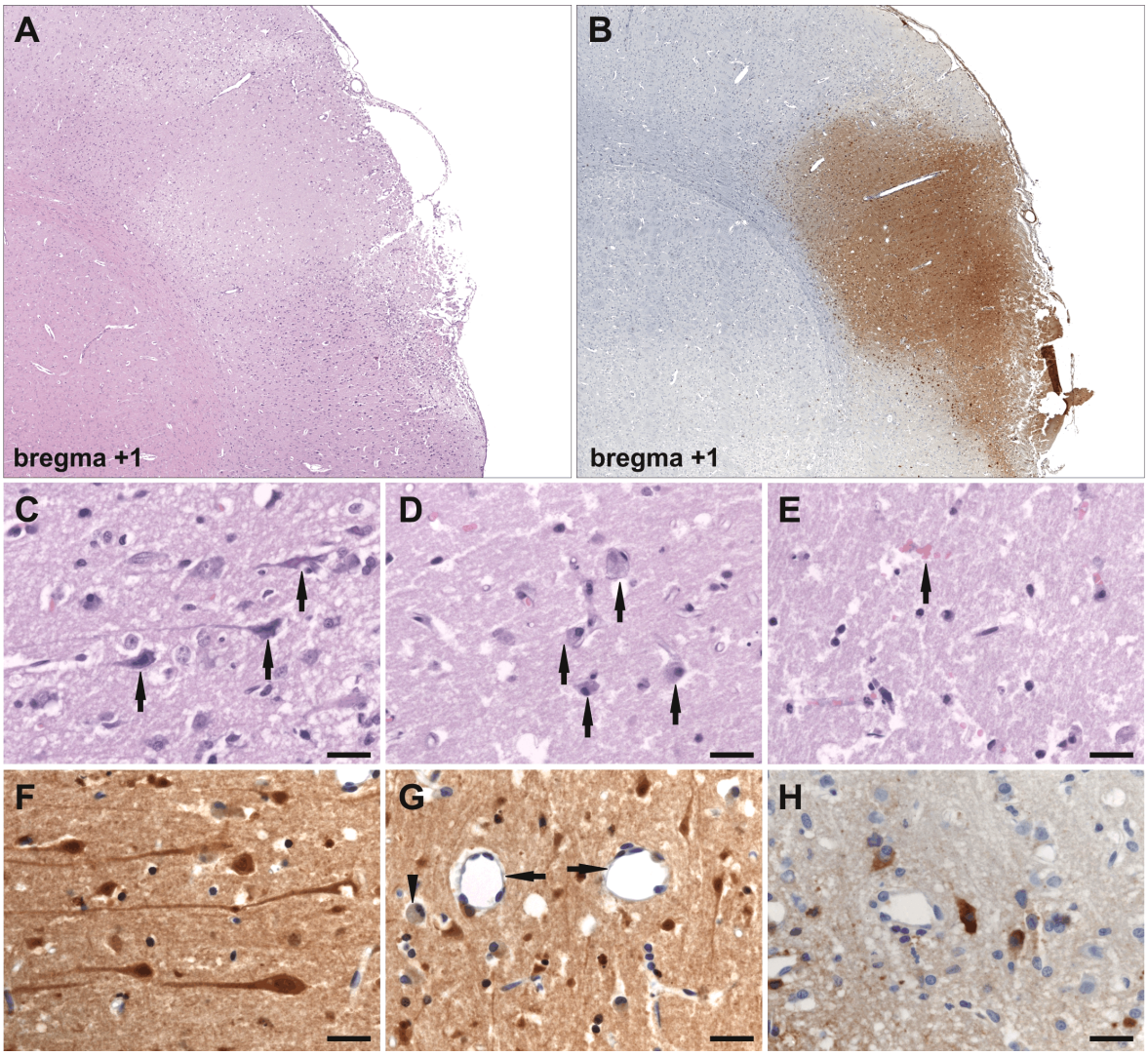

Figure 2 – ***Histopathological (A, C–E) and immunohistochemical (F, G–H) confirmation of the infarct area exemplary image on an untreated rat at the coronal level bregma +1 mm. Shrinked, eosinophilic neurons (arrows in A) with irreversible nuclear changes (arrows in B) accumulation of foamy macrophages and (arrow in C) minimal petechial red blood cells extravasation characterize these animals. Immunostaining for GAP-43 labels the (F) perikarya, their apical dendrites, and to a lesser extent glial-like cells, with (G) a relative sparring of the endothelial cells (arrows) and foamy macrophages (arrowhead). Around the infarct core (H) a few labeled neurons are also detectable on the background of a non-stained neuropil. Scale bars represent 20 µm.***

Using Cavalieri's principle, volumetric data calculated on a region of 250×15 = 3.750 µm starting from the +2 bregma level encompassed the whole infarct cores (Figure 3, A–D). Ipsilateral (per-infarct) hemisphere volumes were significantly higher in MCAO untreated animals (995.10± 71.42 mm^3) compared to MCAO treated (851.05±54.2 mm^3) animals ($p<0.01$) and to sham volumes (766.92±56.26 mm^3) ($p<0.01$) (Figure 3D). The contralateral hemispheres also had higher volumes in MCAO untreated animals (894.27± 71.42 mm^3) compared to treated (808.87±61.8 mm^3) and sham animals ($p<0.05$, respectively $p<0.01$). There was no significant difference between the MCAO treated contralateral hemisphere and the sham animals. The infarct cores themselves, as delineated by GAP-43 reactivity, showed a small but significant increase in MCAO untreated (129.05±22.36 mm^3) *versus* treated animals (97.25±21.34 mm^3) ($p<0.05$).

Three-dimensional surface scanning was deemed reproducible, since after repositioning the specimen and re-scanning it, a paired T testing showed no significant differences between the results for the three groups of data ($p<0.05$ for repeated measurements of MCAO treated, MCAO untreated and sham animals). Total volumetric analysis extracted from 3D surface scanning revealed higher total volumes in MCAO untreated animals (2018.25± 115.24 mm^3) compared to untreated (1798.45±115.24 mm^3) ($p<0.01$) and sham animals (1742.21±96.21 mm^3) ($p<0.01$) (Figure 4). There was no difference between treated and sham animals, although there was a tendency for the treated animals to exhibit higher volume values.

There was a very strong direct correlation between the ipsilateral hemisphere volumes and the infarct core volumes [$r(4)=0.842$, $p<0.05$], with a strong direct correlation between the contralateral hemisphere volumes and the infarct core volumes [$r(4)=0.684$, $p<0.05$]. Also, a very strong direct correlation was deemed between the ipsilateral hemisphere volumes/infarct core volumes and the total telencephalic-diencephalic volumes [$r(4)=0.853$, $p<0.01$], respectively [$r(4)=0.714$, $p<0.05$].

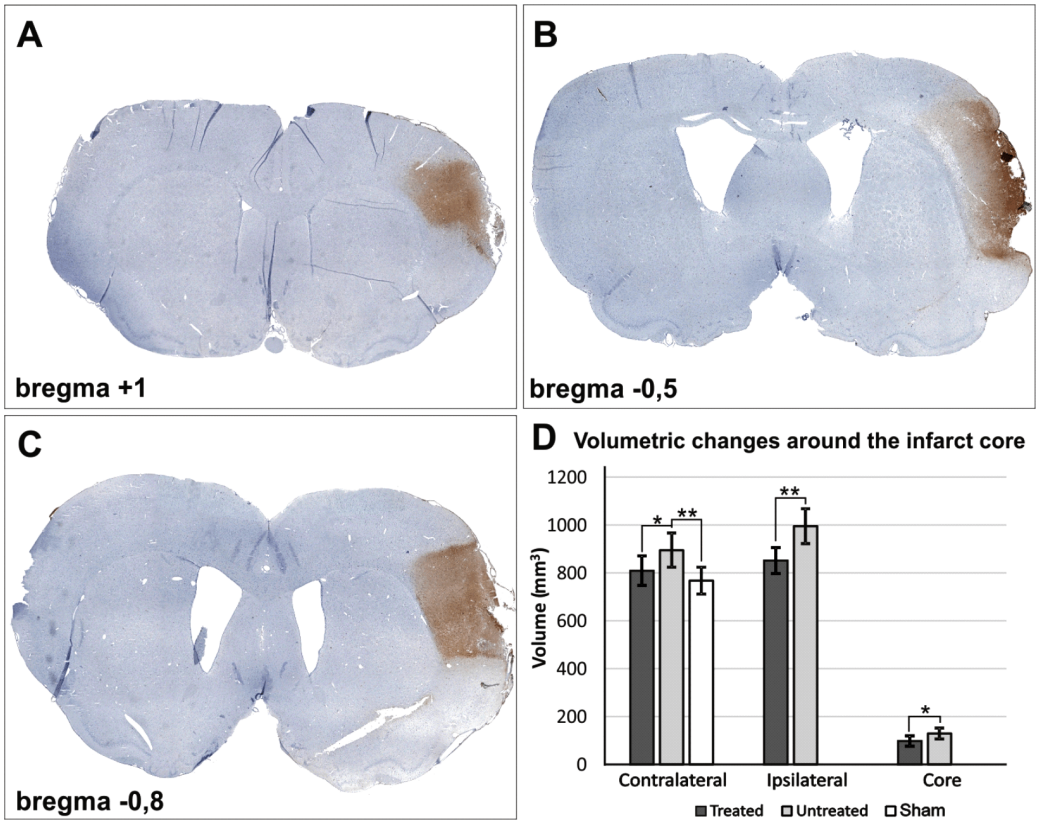

Figure 3 – ***Exemplary images of whole slide scans (immunohistochemistry for GAP-43, TGN-020 treated rat) utilized to calculate the individual hemisphere/infarct areas and to extrapolate tissue volumes utilizing Cavalieri's principle (A–C). (D) TGN-020 treated animals show a clear-cut reduction of both hemispheres' volume, and of the infarct cores' volume, while not showing anymore a significant difference for the sham animals versus the contralateral hemispheres of treated animals. Data are expressed as means ± SD, *p<0.05, **p<0.01 using one-way ANOVA followed by a Fisher's LSD significant difference testing (HSD) test, n=5–6/group. LSD: Least significant difference; HSD: Honest significant difference.***

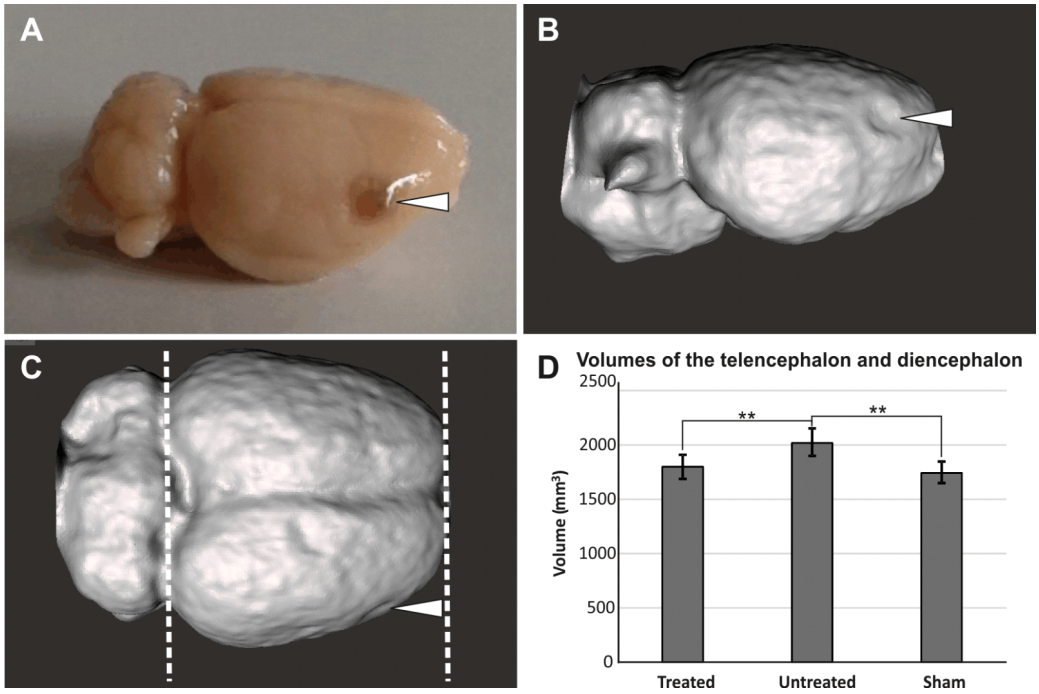

Figure 4 – ***Exemplary images of a dissected perfused brain (untreated animal) (A) and ex vivo three-dimensional scan results of the same tissue (B–D). Surface rendering (B) allows the visualization of the infarct core, and (C) selection of only the telencephalon for further volumetric analysis. (D) Total telencephalon analysis shows significantly higher brain volumes for untreated animals compared to treated and sham animals. Data are expressed as means ± SD, **p<0.01 using one-way ANOVA followed by a Fisher's LSD significant difference testing (HSD) test, n=5–6/group. LSD: Least significant difference; HSD: Honest significant difference.***

Discussion

Aquaporins (AQPs) constitute ubiquitous transmembrane channels that drive the passive diffusion of water and small solutes between the cells following local osmotic gradients. There are 12 aquaporin family members in humans, and they are essentially implicated in almost all fluid dynamics in the body [24, 25]. In the kidneys, they are responsible for concentrating the urine [26], they drive the secretion of water into glandular acini leading to sweat, saliva, mucus and tears production [27, 28], they are as well present in the ciliary epithelium of the choroid leading to aqueous humor secretion into the posterior chamber of the eye [29], and they contribute to acid secretion by gastric parietal cells [30].

The brain is no exception from this rule, and AQP4 and AQP1 are responsible for most of the water diffusion in the brain and spinal cord. Thus, AQP4 is known to be expressed and active at the level of the overall astrocyte membrane, especially on the perivascular end-feets, and the inner and outer *glia limitans* [6, 8, 31]. Although present to a less extent than AQP4, AQP1 is mainly expressed at the levels of the choroid plexuses and it has been proposed to be involved in the formation of cerebrospinal fluid [32]. Not only that AQP4 is the key player in maintaining water homeostasis in the brain, but it has also been showed to exhibit clear-cut prone potential as a therapeutic option directly targeting brain edema. First, AQP4 knockout mice with acute hypervolemia and with a focal ischemic stroke produced by MCA occlusion showed significantly decreased cerebral edema formation and improved neurological outcomes compared to counterpart nontransgenic animals [9]. On the other hand, induction of a vasogenic brain edema (intraparenchymal fluid infusion or freeze-injury models) on the same AQP4-/- background results in increased brain volumes and impaired clinical outcomes [33, 34]. Moreover, utilizing small interference RNA targeting AQP4 (siAQP4) leads to a local reduction of AQP4 expression by 30%, and a significant reduction of cerebral edema after brain trauma [35, 36]. The bidirectional gradient-driven water flow through the AQP4 pores explains the fact that in cytotoxic edema occurring around an intact BBB, AQP4 loss reduces water influx toward the brain, while opening the BBB on the same genetic background reduces the water outflow from the brain.

In these conditions, selective AQP4 inhibitors would represent an attractive treatment option in the initial phases of an ischemic stroke with minimal hemorrhage transformation. A recent study identified 2-(nicotinamide)-1,3,4-thiadiazole (TGN-020) as a potent AQP4 inhibitor [13], and on a mouse model of focal cerebral ischemia, one single pretreatment with TGN-020 before the induction of ischemia significantly reduced brain edema without any detectable histopathological side effects [14]. The same compound has been further utilized as a reporter for *in vivo* positron emission tomography (PET) imaging of AQP4 [19]. However, to date no direct histopathological evidence for the reduction of the infarct size after TGN-020 administration on an MCAO model has been published.

GAP-43 is a 43-kDa protein expressed at increased levels in the developing and regenerating neurons, in the so-called axon growth cones [37]. This membrane neuron-specific protein is sought to be expressed during axon regeneration while being absent from the dendritic growth cones [37]. Acute aberrant regenerative signaling after cortical ischemia have been reported to increase the expression of GAP-43 in the adult central nervous system (CNS), making it a suitable marker for axonal and regenerative response in the ischemic area [38–40].

We have evaluated here for the first time the direct histopathological effect of a single intraperitoneal dose of TGN-020 administrated at short time after inducing cerebral ischemia, on a rat model of ischemic stroke. Immunohistochemistry for GAP-43 allowed us to clearly delineate and measure the areas of infarcted tissue, and together with a systematic slide sampling at known distances, we could directly asses brain and infarct volumes on a brain slice with a thickness of 3750 μm (15 sections at 250 μm apart), utilizing the Cavalieri method of volumetric estimation [41]. Ipsilateral hemisphere volumes were clearly increased in MCAO untreated animals compared to sham and both hemispheres of the TGN-020 treated animals. The effect was also present in the contralateral hemisphere, to a lesser extent, bust still with a significant difference from the untreated animals. Essentially, the infarct core itself was clearly reduced in treated animals *versus* MCAO untreated animals.

Next, we have utilized for the first time a 3D scanner to obtain real *ex vivo* volumetric data of the investigated brains. Although as it was based on the direct investigation of the surface of the brains, and this procedure was not capable of evaluating the volumes of the infarct cores, it could offer precise whole-telencephalon volumetric data. Replicated measurements provided volumetric values with non-significant differences between the repeated data, proving the utility of such a system for tissue macroscopic objective evaluation. Untreated animals showed increased telencephalon volumes compared to treated and sham experiments, while there was no significant difference between treated and sham animals.

Although the effect of TGN-020 has been described on imaging studies when administrated before the MCAO [14], this is the first direct histopathological evidence for the efficiency of TGN-020 when administrated after induction of the ischemia, providing one more step towards its utility as a clear-cut treatment option of the initial phases of ischemic stroke.

The main limitations of the study came from the small number of available animals, which resulted from the price of TGN-020 salt, and the fact that in contrast to other available studies we have utilized here rats and not mice. However, this fact allowed a better surgical approach of the larger CNS of the rat, and was the main reason for selecting this model. Another limitation came from the fact that we have actually measured *ex vivo* brain volumes after the animals had been perfused with saline and formalin, and we did not have *in vivo* volumetric/imaging data. In this line, we are currently involved in assessing the differences between MRI and *ex vivo* 3D organ scanning, which will be an important confirmation for the object scanning technology.

Conclusions

The conclusion of this study is twofold. First of all, we have provided here the first histopathological evidence of total brain and infarct volume reduction after TGN-020 AQP4 inhibitor administration consecutively to MCAO induction, and second, we have utilized for the first time a high-resolution object scanner in order to asses volumetric changes of the brain.

Conflict of interests

The authors declare that they have no conflict of interests.

Acknowledgments

This work was supported by a grant of the Romanian National Authority for Scientific Research and Innovation, CNCS – UEFISCDI, project number PN-II-RU-TE-2014-4-0582, contract number 160/01.10.2015.

Author contribution

Elena Silvia Popescu, Ionica Pirici and Tudor-Adrian Bălşeanu equally contributed to the manuscript.

References

[1] Writing Group Members, Mozaffarian D, Benjamin EJ, Go AS, Arnett DK, Blaha MJ, Cushman M, Das SR, de Ferranti S, Després JP, Fullerton HJ, Howard VJ, Huffman MD, Isasi CR, Jiménez MC, Judd SE, Kissela BM, Lichtman JH, Lisabeth LD, Liu S, Mackey RH, Magid DJ, McGuire DK, Mohler ER 3rd, Moy CS, Muntner P, Mussolino ME, Nasir K, Neumar RW, Nichol G, Palaniappan L, Pandey DK, Reeves MJ, Rodriguez CJ, Rosamond W, Sorlie PD, Stein J, Towfighi A, Turan TN, Virani SS, Woo D, Yeh RW, Turner MB; American Heart Association Statistics Committee; Stroke Statistics Subcommittee. Executive summary: heart disease and stroke statistics – 2016 update: a report from the American Heart Association. Circulation, 2016, 133(4):447–454.

[2] Mackay JM, Mensah GA. The atlas of heart disease and stroke. World Health Organization, Geneva, 2004.

[3] Roger VL, Go AS, Lloyd-Jones DM, Adams RJ, Berry JD, Brown TM, Carnethon MR, Dai S, de Simone G, Ford ES, Fox CS, Fullerton HJ, Gillespie C, Greenlund KJ, Hailpern SM, Heit JA, Ho PM, Howard VJ, Kissela BM, Kittner SJ, Lackland DT, Lichtman JH, Lisabeth LD, Makuc DM, Marcus GM, Marelli A, Matchar DB, McDermott MM, Meigs JB, Moy CS, Mozaffarian D, Mussolino ME, Nichol G, Paynter NP, Rosamond WD, Sorlie PD, Stafford RS, Turan TN, Turner MB, Wong ND, Wylie-Rosett J; American Heart Association Statistics Committee and Stroke Statistics Subcommittee. Heart disease and stroke statistics – 2011 update: a report from the American Heart Association. Circulation, 2011, 123(4):e18–e209.

[4] Qureshi AI, Suarez JI, Yahia AM, Mohammad Y, Uzun G, Suri MF, Zaidat OO, Ayata C, Ali Z, Wityk RJ. Timing of neurologic deterioration in massive middle cerebral artery infarction: a multicenter review. Crit Care Med, 2003, 31(1): 272–277.

[5] Thrane AS, Rangroo Thrane V, Nedergaard M. Drowning stars: reassessing the role of astrocytes in brain edema. Trends Neurosci, 2014, 37(11):620–628.

[6] Nielsen S, Nagelhus EA, Amiry-Moghaddam M, Bourque C, Agre P, Ottersen OP. Specialized membrane domains for water transport in glial cells: high-resolution immunogold cytochemistry of aquaporin-4 in rat brain. J Neurosci, 1997, 17(1):171–180.

[7] Nagelhus EA, Mathiisen TM, Ottersen OP. Aquaporin-4 in the central nervous system: cellular and subcellular distribution and coexpression with KIR4.1. Neuroscience, 2004, 129(4): 905–913.

[8] Mogoanta L, Ciurea M, Pirici I, Margaritescu C, Simionescu C, Ion DA, Pirici D. Different dynamics of aquaporin 4 and glutamate transporter-1 distribution in the perineuronal and perivascular compartments during ischemic stroke. Brain Pathol, 2014, 24(5):475–493.

[9] Manley GT, Fujimura M, Ma T, Noshita N, Filiz F, Bollen AW, Chan P, Verkman AS. Aquaporin-4 deletion in mice reduces brain edema after acute water intoxication and ischemic stroke. Nat Med, 2000, 6(2):159–163.

[10] Papadopoulos MC, Verkman AS. Aquaporin-4 gene disruption in mice reduces brain swelling and mortality in pneumococcal meningitis. J Biol Chem, 2005, 280(14):13906–13912.

[11] Bloch O, Papadopoulos MC, Manley GT, Verkman AS. Aquaporin-4 gene deletion in mice increases focal edema associated with staphylococcal brain abscess. J Neurochem, 2005, 95(1):254–262.

[12] Bloch O, Auguste KI, Manley GT, Verkman AS. Accelerated progression of kaolin-induced hydrocephalus in aquaporin-4-deficient mice. J Cereb Blood Flow Metab, 2006, 26(12): 1527–1537.

[13] Huber VJ, Tsujita M, Nakada T. Identification of aquaporin 4 inhibitors using *in vitro* and *in silico* methods. Bioorg Med Chem, 2009, 17(1):411–417.

[14] Igarashi H, Huber VJ, Tsujita M, Nakada T. Pretreatment with a novel aquaporin 4 inhibitor, TGN-020, significantly reduces ischemic cerebral edema. Neurol Sci, 2011, 32(1):113–116.

[15] Nakamura Y, Suzuki Y, Tsujita M, Huber VJ, Yamada K, Nakada T. Development of a novel ligand, [C]TGN-020, for aquaporin 4 positron emission tomography imaging. ACS Chem Neurosci, 2011, 2(10):568–571.

[16] Popa-Wagner A, Stöcker K, Balseanu AT, Rogalewski A, Diederich K, Minnerup J, Margaritescu C, Schäbitz WR. Effects of granulocyte-colony stimulating factor after stroke in aged rats. Stroke, 2010, 41(5):1027–1031.

[17] Llovera G, Roth S, Plesnila N, Veltkamp R, Liesz A. Modeling stroke in mice: permanent coagulation of the distal middle cerebral artery. J Vis Exp, 2014, (89):e51729.

[18] Igarashi H, Tsujita M, Suzuki Y, Kwee IL, Nakada T. Inhibition of aquaporin-4 significantly increases regional cerebral blood flow. Neuroreport, 2013, 24(6):324–328.

[19] Suzuki Y, Nakamura Y, Yamada K, Huber VJ, Tsujita M, Nakada T. Aquaporin-4 positron emission tomography imaging of the human brain: first report. J Neuroimaging, 2013, 23(2): 219–223.

[20] Paxinos G, Watson C. The rat brain in stereotaxic coordinates. 7th edition, Academic Press–Elsevier, London, 2014.

[21] Rosen GD, Harry JD. Brain volume estimation from serial section measurements: a comparison of methodologies. J Neurosci Methods, 1990, 35(2):115–124.

[22] García-Fiñana M, Cruz-Orive LM, Mackay CE, Pakkenberg B, Roberts N. Comparison of MR imaging against physical sectioning to estimate the volume of human cerebral compartments. Neuroimage, 2003, 18(2):505–516.

[23] Gundersen HJ, Jensen EB, Kiêu K, Nielsen J. The efficiency of systematic sampling in stereology – reconsidered. J Microsc, 1999, 193(Pt 3):199–211.

[24] Itoh T, Rai T, Kuwahara M, Ko SB, Uchida S, Sasaki S, Ishibashi K. Identification of a novel aquaporin, AQP12, expressed in pancreatic acinar cells. Biochem Biophys Res Commun, 2005, 330(3):832–838.

[25] Verkman AS, Anderson MO, Papadopoulos MC. Aquaporins: important but elusive drug targets. Nat Rev Drug Discov, 2014, 13(4):259–277.

[26] Ma T, Yang B, Gillespie A, Carlson EJ, Epstein CJ, Verkman AS. Generation and phenotype of a transgenic knockout mouse lacking the mercurial-insensitive water channel aquaporin-4. J Clin Invest, 1997, 100(5):957–962.

[27] Delporte C, Bryla A, Perret J. Aquaporins in salivary glands: from basic research to clinical applications. Int J Mol Sci, 2016, 17(2), pii:E166.

[28] Ma T, Song Y, Gillespie A, Carlson EJ, Epstein CJ, Verkman AS. Defective secretion of saliva in transgenic mice lacking aquaporin-5 water channels. J Biol Chem, 1999, 274(29): 20071–20074.

[29] Zhang D, Vetrivel L, Verkman AS. Aquaporin deletion in mice reduces intraocular pressure and aqueous fluid production. J Gen Physiol, 2002, 119(6):561–569.

[30] Matsuzaki T, Tajika Y, Ablimit A, Aoki T, Hagiwara H, Takata K. Aquaporins in the digestive system. Med Electron Microsc, 2004, 37(2):71–80.

[31] Rash JE, Yasumura T, Hudson CS, Agre P, Nielsen S. Direct immunogold labeling of aquaporin-4 in square arrays of astrocyte and ependymocyte plasma membranes in rat brain and spinal cord. Proc Natl Acad Sci U S A, 1998, 95(20): 11981–11986.

[32] Verkman AS, Mitra AK. Structure and function of aquaporin water channels. Am J Physiol Renal Physiol, 2000, 278(1): F13–F28.
[33] Tait MJ, Saadoun S, Bell BA, Verkman AS, Papadopoulos MC. Increased brain edema in aqp4-null mice in an experimental model of subarachnoid hemorrhage. Neuroscience, 2010, 167(1):60–67.
[34] Papadopoulos MC, Manley GT, Krishna S, Verkman AS. Aquaporin-4 facilitates reabsorption of excess fluid in vasogenic brain edema. FASEB J, 2004, 18(11):1291–1293.
[35] Fukuda AM, Adami A, Pop V, Bellone JA, Coats JS, Hartman RE, Ashwal S, Obenaus A, Badaut J. Posttraumatic reduction of edema with aquaporin-4 RNA interference improves acute and chronic functional recovery. J Cereb Blood Flow Metab, 2013, 33(10):1621–1632.
[36] Badaut J, Ashwal S, Adami A, Tone B, Recker R, Spagnoli D, Ternon B, Obenaus A. Brain water mobility decreases after astrocytic aquaporin-4 inhibition using RNA interference. J Cereb Blood Flow Metab, 2011, 31(3):819–831.
[37] Goslin K, Schreyer DJ, Skene JH, Banker G. Development of neuronal polarity: GAP-43 distinguishes axonal from dendritic growth cones. Nature, 1988, 336(6200):672–674.
[38] Li Y, Jiang N, Powers C, Chopp M. Neuronal damage and plasticity identified by microtubule-associated protein 2, growth-associated protein 43, and cyclin D1 immunoreactivity after focal cerebral ischemia in rats. Stroke, 1998, 29(9):1972–1980; discussion 1980–1981.
[39] Aigner L, Arber S, Kapfhammer JP, Laux T, Schneider C, Botteri F, Brenner HR, Caroni P. Overexpression of the neural growth-associated protein GAP-43 induces nerve sprouting in the adult nervous system of transgenic mice. Cell, 1995, 83(2):269–278.
[40] Stroemer RP, Kent TA, Hulsebosch CE. Acute increase in expression of growth associated protein GAP-43 following cortical ischemia in rat. Neurosci Lett, 1993, 162(1–2):51–54.
[41] Pirici I, Ciurea ME, Mîndrilă I, Avrămoiu I, Pirici A, Nicola MG, Rogoveanu OC. Basal cell carcinoma develops in contact with the epidermal basal cell layer – a three-dimensional morphological study. Rom J Morphol Embryol, 2016, 57(1):99–105.

Corresponding author
Raluca Niculina Ciurea, Associate Professor, MD, PhD, Department of Pathology, University of Medicine and Pharmacy of Craiova, 2 Petru Rareş Street, 200349 Craiova, Dolj County, Romania; Phone +40735–224 333, e-mail: raluca1ciurea@gmail.com

Received: March 9, 2016

Accepted: January 3, 2017